Letters

A Switchable-*LCL*-Circuit-Based IPT System With High Efficiency for Reefer Containers

Yefei Xu, Ruikun Mai, *Senior Member, IEEE*, Wei Liu, Shuaishuai Pan, Yang Chen, *Member, IEEE*, Zhengyou He, *Senior Member, IEEE*, Yong Li, *Member, IEEE*, and Udaya Kumara Madawala, *Fellow, IEEE*

***Abstract*—To get rid of plug-in/out actions for automatic wharves, a switchable-*LCL*-circuit (SLC) based inductive power transfer system is proposed to improve efficiency for reefer container wireless charging. As we knew, the power requirement of a reefer container only hits a few operation points, and each operation point is in corresponding to an individual resistance point (IRP). Therefore, the system efficiency can be improved by altering the IRPs into the optimal load resistance (OLR). The idea of this letter is to use the SLC to create multiple efficiency-load curves, then to regulate the peak points of the curves approaching the IRPs by reconfiguring the compensation parameters. Finally, a prototype was built to validate the performance of the proposed approach. The experimental results show that with the SLC, both the IRPs 20 and 160 Ω can be transformed into the OLR 55 Ω; the proposed system can gain the system efficiency >92.4% at the IRPs (20 Ω, 259.2 W) and (160 Ω, 32.4 W).**

***Index Terms*—Efficiency optimization, inductive power transfer (IPT), *LCL* circuit.**

I. Introduction

REEFER containers play an essential role in the cold-chain transportation industry. Nowadays, the reefer containers are powered by plug-in systems, which suffer from following three main drawbacks.

1) The physical plug-in connection is labor intensive and time consuming, and also prone to undesirable unplugging when containers are moved, leading to equipment damage.
2) Such systems are not ideal for operation under adverse weather conditions, such as rain and snow etc.
3) Most of the operations in automatic wharves can be done by the automatic machines except plugging-in/out the cables of the reefer containers.

Thus, the engineers desire to find a solution to achieve a completely automatic wharf. These drawbacks can be alleviated by wirelessly powering these containers using wireless inductive power transfer (IPT) technology. IPT facilitates electrical power transfer over an air-gap through magnetic coupling without any direct electrical connections, and has been employed in many industrial applications, such as wearable devices [1], automatic guided auto [2], electrical vehicles [3]–[6], and railways [7]. Thus, IPT technology is hoped to offer an expandable option for reefer container charging. Fig. 1 shows plug-in systems and IPT systems for reefer containers.

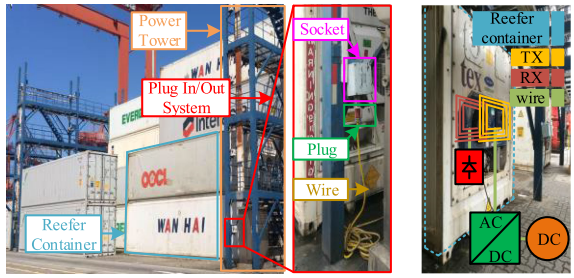

Fig. 1. (a) Reefer containers and power tower. (b) Installation of an IPT system for a reefer container.

As for many other applications, the efficiency of power transfer is also of great importance to reefer containers. The system efficiency varies with the load, and is usually optimized only for a particular load, referred hereafter as the optimal load resistance (OLR). Unfortunately, each reefer container operates under three different conditions and, thus, invariably appears as a variable load to the power transfer system. The three typical loading conditions of reefer containers, represented as individual resistance points (IRPs), are listed in Table I.

To deliver power with high efficiency in a large load resistance range, power converters, e.g., dc–dc converters and active rectifiers, are widely used to adaptively change the load impedance to achieve impedance matching for maximum efficiency point tracking [8]–[10]. These methods can optimize efficiency

Manuscript received April 29, 2020; revised June 12, 2020; accepted July 6, 2020. Date of publication July 17, 2020; date of current version September 22, 2020. This work was supported in part by the National Natural Science Foundation of China under Grants 51677155 and 51907169, in part by the International Science and Technology Innovation Cooperation Program of Sichuan Province under Grant 2020YFH0031, and in part by the Fundamental Research Funds for the Central Universities under Grant 2682020CX16. *(Corresponding author: Ruikun Mai.)*

Yefei Xu, Ruikun Mai, Wei Liu, Shuaishuai Pan, Yang Chen, Zhengyou He, and Yong Li are with the School of Electrical Engineering, Southwest Jiaotong University, Chengdu 611756, China (e-mail: xuyefei1991@foxmail.com; mairk@swjtu.edu.cn; 474391501@qq.com; panshuai626@163.com; yangchen@swjtu.edu.cn; hezy@home.swjtu.edu.cn; leeo1864@163.com).

Udaya Kumara Madawala is with the University of Auckland, Auckland 1142, New Zealand (e-mail: u.madawala@auckland.ac.nz).

Color versions of one or more of the figures in this letter are available online at https://ieeexplore.ieee.org.

Digital Object Identifier 10.1109/TPEL.2020.3010012

TABLE I
RESISTANCE OF A TYPICAL REEFER CONTAINER

Operating status	Power	Resistance point
Refrigeration	6.6kW	22Ω
Heating	3.0kW	48Ω
air recirculation/defrosting	≈1.5kW	96Ω

dramatically. However, some extra power loss, e.g., switch loss, is introduced by the power converters. Tuning operating frequency is another effective way [11]. Nevertheless, this method is limited by the Industrial Scientific Medical band. Tunable capacitors, which are derived by a step motor, are utilized in [12]. However, the auxiliary control circuit is complicated.

Recently, switchable circuits (SCs) have also been proposed to improve system efficiency. The idea of the SCs is to use switches to alter system parameters or topologies to create multiple efficiency-load curves, then to control the system operating within the top regions of the curves. Using switchable capacitor and/or inductor matrixes is a valid approach [13], [14]. However, lots of passive components and switches increase the circuit complexity. Thus, the fewer the components and switches are required for creating one more efficiency curve, the better the performance of the SCs is. Therefore, Kim and Jeong [15] and Dang *et al.* [16] use several combinations of switches and subcoils to change mutual inductances; Mai *et al.* [17] and Zhong and Hui [18] use two or three switches to alter system topologies with splitting coils. However, reactive power, which is harmful to the IPT system, is introduced. Moreover, the specially designed sub- or splitting coils complicates the system design.

The methods mentioned earlier focus on improving the system efficiency in a continuous load resistance range. However, the load resistances of a reefer container vary discretely among a few IRPs. Therefore, for the reefer container application, only the system efficiency at the IRPs is required to be optimized. In this letter, a switchable-*LCL*-circuit (SLC) based IPT system is proposed for the reefer container wireless charging. Compared with the traditional SCs, the main advantages of the SLC are as follows.

1) Only a switch, an inductor, and a capacitor are required for creating one more efficiency-load curve without introducing any reactive power.
2) The coil design is easy with the SLC because the specially designed coils are not required.

II. OPTIMAL IMPEDANCE MATCHING BY *LCL* CIRCUIT

A. OLR of a Series–Series (SS) IPT System

According to Zhong and Hui [9], for a given SS IPT system, the OLR R_{Lopt}, which can achieve the optimal efficiency η_{opt}, can be expressed as

$$R_{\mathrm{Lopt}} = \left[\sqrt{R_{\mathrm{P}}R_{\mathrm{S}}(\omega M)^2 + (R_{\mathrm{P}}R_{\mathrm{S}})^2}\right]/R_{\mathrm{P}} \tag{1}$$

where $R_{\mathrm{P}} = R_{\mathrm{LP}}+R_{\mathrm{CP}}$, $R_{\mathrm{S}} = R_{\mathrm{LS}}+R_{\mathrm{CS}}$. R_{LP}, R_{LS}, R_{CP}, and R_{CS} are the equivalent series resistors (ESRs) of the transmitting coil L_{P}, the receiving coil L_{S}, and the compensation capacities C_{P} and C_{S}, respectively. M denotes the mutual inductance between L_{P} and L_{S}. ω is the operating angular frequency. When the load resistance R_{L} deviates from R_{Lopt}, the system efficiency will decrease.

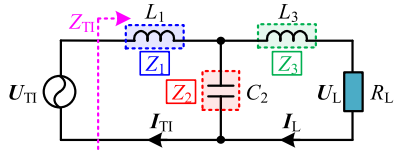

Fig. 2. Circuit model of a general *LCL* circuit.

B. Analysis of LCL Circuit

A general *LCL* circuit consists of an ac power source U_{TI}, an ac load R_{L}, two inductors L_1, L_3, and a capacitor C_2, as shown in Fig. 2. $\boldsymbol{U_{\mathrm{TI}}}$ ($\boldsymbol{U_{\mathrm{L}}}$) is the phasor of the source (load) voltage U_{TI} (U_{L}). $\boldsymbol{I_{\mathrm{TI}}}$ ($\boldsymbol{I_{\mathrm{L}}}$) is the phasor of the source (load) current I_{TI} (I_{L}). Z_1, Z_2, and Z_3 are the impedances of L_1, C_2, and L_3, respectively. The *LCL* circuit is designed to operate at ω. Thus, we can obtain

$$Z_2 = -Z_1, \quad Z_3 = Z_1. \tag{2}$$

According to Kirchhoff's voltage law, the circuit can be described as

$$\begin{bmatrix} \boldsymbol{U}_{\mathrm{TI}} \\ 0 \end{bmatrix} = \begin{bmatrix} Z_1+Z_2 & -Z_2 \\ -Z_2 & Z_2+Z_3+R_{\mathrm{L}} \end{bmatrix} \cdot \begin{bmatrix} \boldsymbol{I}_{\mathrm{TI}} \\ \boldsymbol{I}_{\mathrm{L}} \end{bmatrix}. \tag{3}$$

By substituting (2) into (3), and solving (3), Z_{TI}, the input impedance of the *LCL* circuit, is derived as

$$Z_{\mathrm{TI}} = -{Z_1}^2/R_{\mathrm{L}}. \tag{4}$$

By adopting a proper Z_1, R_{L} is transformed into Z_{TI}, which can be a smaller or larger value than R_{L}. Besides, Z_{TI} only consists of a real part. Thus, the circuit does not introduce reactive power.

C. Transformation of IRP to OLR

According to (4), to transform R_{L} into R_{Lopt}, namely $Z_{\mathrm{TI}} = R_{\mathrm{Lopt}}$, Z_1 should satisfy the equation as follows:

$$Z_1 = \sqrt{-R_{\mathrm{L}}R_{\mathrm{Lopt}}}. \tag{5}$$

For a given *LCL* circuit, Z_1 is constant. Thus, only a given R_{L} can be transformed into R_{Lopt}. However, the load resistance $R_{\mathrm{L}n}$ of a reefer container varies among several IRPs $\boldsymbol{R_{\mathrm{L}}} = \{R_{\mathrm{L}1}, R_{\mathrm{L}2}, \ldots, R_{\mathrm{L}N}\}$ (N is the number of the IRPs). Thus, η_{opt} cannot always be achieved. To maintain η_{opt}, Z_1 should be dynamically regulated to a proper value in corresponding to $R_{\mathrm{L}n}$.

III. OPTIMAL IMPEDANCE MATCHING BY SLC

A. Analysis of SLC

To transform any $R_{\mathrm{L}n} \in \boldsymbol{R_{\mathrm{L}}}$ into R_{Lopt}, the corresponding SLC is proposed in Fig. 3. C_2 and L_3 of the *LCL* circuit in Fig. 2 are divided into N parts, $C_{2,1}$–$C_{2,N}$ and $L_{3,1}$–$L_{3,N}$. The capacitor

$C_{2,i}$ $(1 \le i \le N)$ is compensated by the inductor $L_{3,i}$. Switches S_1–S_N are utilized to alter the topology of the SLC. There must be one and only one switch being on at any time.

When the switch S_n $(1 \le n \le N)$ is ON, the impedances of the three branches of the SLC can be expressed as

$$Z_{1,n} = j\omega L_1 + \sum_{i=n+1}^{N} \frac{1}{j\omega C_{2,i}} \tag{6}$$

$$Z_{2,n} = \sum_{i=1}^{n} \frac{1}{j\omega C_{2,i}} \tag{7}$$

$$Z_{3,n} = \sum_{i=1}^{n} j\omega L_{3,n}. \tag{8}$$

The SLC is designed to operate at ω. Then, we can obtain

$$Z_{2,n} = -Z_{1,n}, \quad Z_{3,n} = Z_{1,n}. \tag{9}$$

By combining (6)–(9), L_1, $C_{2,1}$–$C_{2,N}$, and $L_{3,1}$–$L_{\mathrm{L}3,N}$ can be solved as

$$L_1 = Z_{1,N}/(j\omega) \tag{10}$$

$$L_{3,i} = \begin{cases} Z_{1,1}/(j\omega) & i = 1 \\ \left[Z_{1,i} - Z_{1,(i-1)}\right]/(j\omega) & i \in [2, N] \end{cases} \tag{11}$$

$$C_{2,i} = \begin{cases} -1/(j\omega Z_{1,1}) & i = 1 \\ -1/\left\{j\omega\left[Z_{1,i} - Z_{1,(i-1)}\right]\right\} & i \in [2, N] \end{cases}. \tag{12}$$

Only a switch S_n, a capacitor $C_{2,n}$, and an inductor $L_{\mathrm{L}3,n}$ are needed to provide one more efficiency curve where IRP $R_{\mathrm{L}n}$ is transformed into R_{Lopt}. When the switch S_n $(1 \le n \le N)$ is ON, to transform $R_{\mathrm{L}n}$ into R_{Lopt}, $Z_{1,n}$ should satisfy the following equation:

$$Z_{1,n} = j\sqrt{R_{\mathrm{Lopt}} R_{\mathrm{L}n}}. \tag{13}$$

B. Design of the SLC-Based IPT System

The aforementioned analysis is ideal without considering the ESRs of the components of the SLC, but it delivers the basic idea of this letter. For the optimization design of a proposed SLC-based IPT system, a precise efficiency model is built. An example of the proposed system ($N = 2$), as shown in Fig. 4(a), mainly consists of a dc voltage source, a high-frequency inverter, a proposed SLC, a rectifier, L_{P}, L_{S}, C_{P}, $C_{\mathrm{S}2}$, and a dc load R_{LDC}. R_{LDC} and R_{L} satisfy

$$R_{\mathrm{LDC}} = (\pi^2 R_{\mathrm{L}})/8. \tag{14}$$

L_1 shown in Fig. 3 is replaced by the combination of L_{S} and $C_{\mathrm{S}2}$, where

$$C_{\mathrm{S}2} = 1/\left(\omega^2 L_{\mathrm{S}} - \omega^2 L_1\right). \tag{15}$$

The circuit model of the system is shown in Fig. 4(b). R_{DS} is the equivalent on-state resistance of the inverter MOSFETs, and U_{D} is the forward voltage of the rectifier diode. $R_{\mathrm{Z}1,n}$, $R_{\mathrm{Z}2,n}$, $R_{\mathrm{Z}3,n}$, and $R_{\mathrm{S}n}$ are the ESRs of $Z_{1,n}$, $Z_{2,n}$, $Z_{3,n}$, and S_n, respectively. U_{IN} (U_{P}) is the input (output) voltage of the inverter. U_{L} (U_{OUT}) is the input (output) voltage of the rectifier.

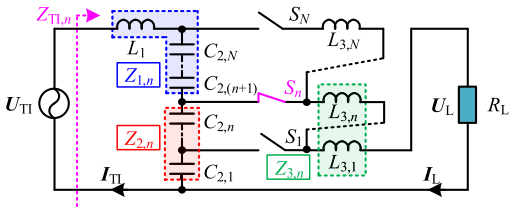

Fig. 3. Circuit model of the proposed SLC.

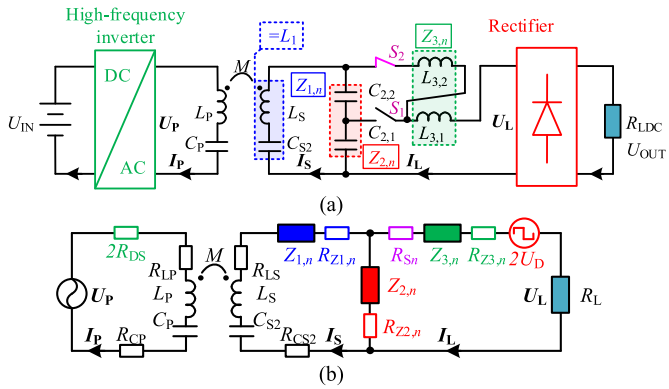

Fig. 4. SLC-based IPT system. (a) System. (b) Circuit model.

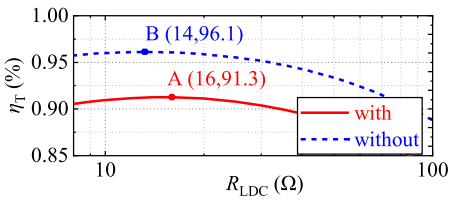

Fig. 5. Calculated system efficiency with/without considering the power losses caused by the inverter, the SLC, and the rectifier (the parameters for the calculation are list in Table II).

I_{P}, I_{S}, and I_{L} are the currents carried by L_{P}, L_{S}, and Z_{3n}, respectively. $\boldsymbol{U_{\mathrm{P}}}$, $\boldsymbol{U_{\mathrm{L}}}$, $\boldsymbol{I_{\mathrm{P}}}$, $\boldsymbol{I_{\mathrm{S}}}$, and $\boldsymbol{I_{\mathrm{L}}}$ are the phasors of U_{P}, U_{L}, I_{P}, I_{S}, and I_{L}, respectively.

The efficiency η_{T} of the proposed system can be expressed as

$$\eta_{\mathrm{T}} = P_{\mathrm{L}}/(P_{\mathrm{DS}} + P_{\mathrm{P}} + P_{\mathrm{S}} + P_{\mathrm{T}} + P_{\mathrm{D}} + P_{\mathrm{L}}) \tag{16}$$

where P_{L} is the load power, and P_{DS}, P_{P}, P_{S}, P_{T}, and P_{D} are the power losses caused by the inverter, the transmitting coil, the receiving coil, the SLC, and the rectifier, respectively. P_{L}, P_{DS}, P_{P}, P_{S}, P_{T}, and P_{D} can be calculated according to Chen *et al.* [19]. In the calculation, the ESRs of the switches are considered as a constant resistance. The ESR $R_{\mathrm{L}x}$ ($R_{\mathrm{C}x}$) of the inductor L_x (capacitor C_x) of the SLC is estimated by assuming that the quality factor of the inductor (capacitor) is Q_{L} (Q_{C})

$$R_{\mathrm{L}x} = \omega L_x/Q_{\mathrm{L}}, R_{\mathrm{C}x} = 1/(\omega C_x Q_{\mathrm{C}}). \tag{17}$$

In Fig. 5, the peak points A and B of the efficiency curves are impacted by P_{DS}, P_{T}, and P_{D}. Thus, considering the power

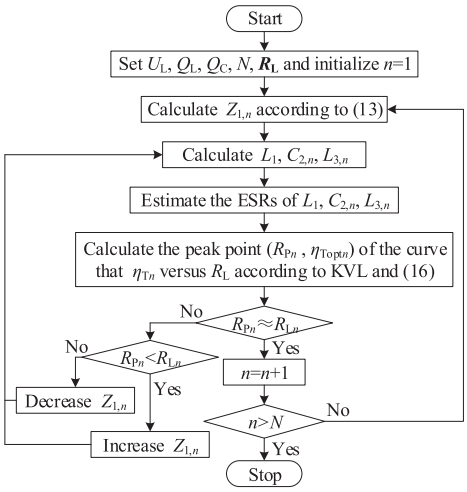

Fig. 6. Design process of the proposed system.

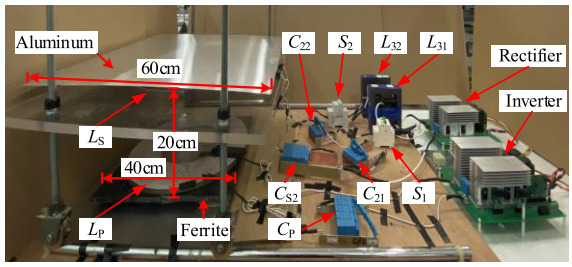

Fig. 7. Prototype of the proposed SLC-based IPT system.

losses can help to achieve a precise design of the proposed system.

According to the aforementioned analysis, we can add a curve η_{Tn} versus R_L by adding a switch S_n, a capacitor $C_{2,n}$, and an inductor $L_{L3,n}$; the peak point (R_{Pn}, η_{Toptn}) of the curve can be shifted by regulating $Z_{1,n}$. Thus, based on a given SS IPT system, the SLC design method is shown in Fig. 6.

IV. Experiment

A. Experiment Prototype

The system in Fig. 4(a) is carried out to verify the theoretical analysis, as shown in Fig. 7. Two air circuit breakers are used as the switches. Two aluminum sheets are applied to reduce the leakage of the electromagnetic field. The airgap is 20 cm. The design and measured parameters of the system are listed in Table II.

B. Experimental Results

In the experiment, U_{IN} is regulated to keep U_{OUT} = 72 V. Fig. 8 shows the experimental waveforms of $\boldsymbol{U_P}$, $\boldsymbol{I_P}$, $\boldsymbol{U_L}$, and $\boldsymbol{I_L}$. When R_{LDC} varies, ($\boldsymbol{U_P}$ and $\boldsymbol{I_P}$) and ($\boldsymbol{U_L}$ and $\boldsymbol{I_L}$) maintain in the same phase, the system keeps resonant, and no reactive power is introduced.

Fig. 9 shows the system efficiency η_S and U_{IN} versus R_{LDC} (η_S here is defined as the ratio of the load power P_L to the input power P_{IN} of the inverter). When S_1 is ON, η_{Topt1} is achieved at 18 Ω, which is near to R_{LDC1} = 20 Ω (259.2 W) and smaller than the original optimal dc load resistance R_{LDCopt} = 55 Ω [R_{LDCopt} is calculated according to (1), (14), and (16)]; when S_2 is ON, η_{Topt2} is achieved at 160 Ω, which is equal to R_{LDC2} = 160 Ω (32.4 W) and is larger than R_{LDCopt}. It indicates that with the proposed SLC, a given R_L, a larger or smaller resistance than R_{Lopt}, can be transformed into R_{Lopt}. When R_{LDC} = 20 Ω (160 Ω), η_S with S_1 (S_2) ON is 92.4% (93.4%), 8.1% (13.3%) higher than η_S with S_2 (S_1) ON. Besides, if the switches are altered at 45 Ω, the proposed system can maintain η_S>90.0% with R_{LDC}∈[8, 500] Ω. Fig. 11 shows the power losses of the proposed system.

TABLE II
Parameters of the Proposed ITP System for the Experiment

Parameter	Value	Parameter	Value	Parameter	Value
U_L	72V	L_{31}	30.9μH	R_{L32}	54.6mΩ
Q_L	600	L_{32}	67.3μH	R_{CP}	8.3mΩ
Q_C	5000	C_P	5.08nF	R_{CS2}	5.2mΩ
N	2	C_{S2}	6.23nF	R_{C21}	41.8mΩ
$\boldsymbol{R_{LDC}}$	{20, 160}Ω	C_{21}	81.67nF	R_{C22}	19.4mΩ
f	100kHz	C_{22}	37.47nF	R_{S1}	8mΩ
M	58.8μH	R_{LP}	372mΩ	R_{S2}	8mΩ
L_P	495.6μH	R_{LS}	382mΩ	R_{DS}	80mΩ
L_S	503.4μH	R_{L31}	33.9mΩ	U_D	1.4V

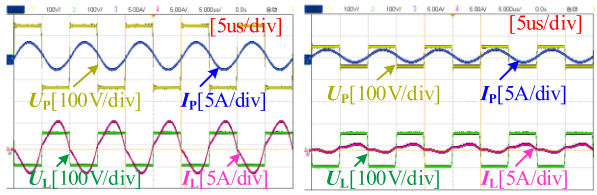

Fig. 8. Experimental waveforms. (a) S_1 ON, R_{LDC} = 20 Ω. (b) S_2 ON, R_{LDC} = 160 Ω.

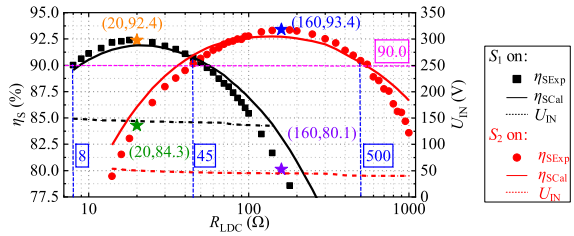

Fig. 9. η_S and U_{IN} versus R_{LDC} (η_{SExp} is a measured efficiency; η_{SCal} is a calculated efficiency with considering the power losses of the inverter, the rectifier, R_{LP}, R_{LS}, R_{L31}, R_{L32}, R_{CP}, R_{CS2}, R_{C21}, R_{C22}, R_{S1}, and R_{S2}).

C. Discuss

Fig. 10 shows the transient process when the switches are altered. The whole process takes about 3.4 s and has a little adverse impact on the reefer containers for which cutting off the power supply for such a short term is admitted.

When S_1 (S_2) is ON, R_{LDC} = 20 Ω (160 Ω), the calculated efficiency η_{SLC} of the SLC is about 99.24% (99.72%), which

TABLE III
COMPARISON AMONG DIFFERENT WORKS

Proposed in	[13]	[14]	[15]	[16]	[17]	[18]	This work
Frequency	13.56MHz	13.56MHz	13.56MHz	8~12MHz	85kHz	100kHz	100kHz
Transmitter coil	400mm	300mm	19~68cm	60cm	20cm	310mm	40cm
Receiver coil	400mm	300mm	19~68cm	60cm	20cm	310mm	40cm
Air gap	0~80cm	6~43cm	10~100cm	0~200cm	7.6cm	85mm	20cm
Coupling coefficient	/	0.05~0.25	/	0.1/0~1	0.2	0.179	0.118
Load resistance	/	/	/	/	30~500Ω	0.82~223Ω	8~500Ω
Output Power	Max 1W	Max 8W	Max 50mW	/	110~420W	Max 10W	10~648W
Efficiency	38~88%	85%	48%~92%	4.9~90%	94.5~95.3%	89~92.6%	90.0~93.4%
Total number of switches	7	23	8	12	2	3	2
Total number of capacitors	11	21	10	2	3	5	4
Total number of inductors/coils	1	4	10	14	4	3	4
Number of switches for creating one more curve	$(\log_2 n)/n$	$2[\log_2(n+1)]/n$	1	1	1	≥1	1
Number of capacitors for creating one more curve	$(\log_2 n)/n$	$2[\log_2(n+1)]/n$	1	0	0.5	≥1	1
Number of inductors/coils for creating one more curve	0	/	1	1	1	≤1	1
VSPD (W/dm^3)	0.67	6.26	0.02	/	342.02	52.08	134.66
GSPD (W/kg)	1.68	17.20	0.04	/	101.94	22.78	49.70
R_{VA}	/	/	/	/	0.029	0.010	0.017
Specially designed coils	No	No	Yes	Yes	Yes	Yes	No
Reactive power	Yes	Yes	Yes	Yes	Yes	Yes	No

Note: n is the total number of the efficiency-load curves.

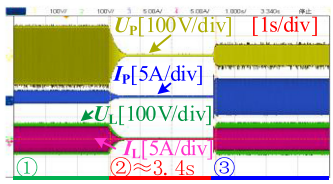

Fig. 10. Transient process at $R_{\mathrm{LDC}} = 45\ \Omega$ (① S_1 ON, S_2 OFF; ② first, turn OFF the dc voltage source; second, turn S_1 OFF, turn S_2 ON; and last, turn ON the dc voltage source; and ③ S_1 OFF, S_2 ON).

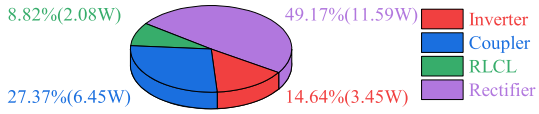

Fig. 11. Calculated power losses of the proposed system (S_1 ON, $R_{\mathrm{LDC}} = 20\ \Omega$).

is higher than that, e.g., <94% in [8], of a traditional dc–dc converter.

To show the performance of the proposed method, volumetric specific power density (VSPD), gravimetric specific power density (GSPD), and volt-ampere (VA) volume rate R_{VA} are defined as

$$\mathrm{VSPD} = \frac{P_{\mathrm{OUT}}}{V_{\mathrm{total}}};\quad \mathrm{GSPD} = \frac{P_{\mathrm{OUT}}}{G_{\mathrm{total}}};\quad R_{\mathrm{VA}} = \frac{P_{\mathrm{OUT}}}{\mathrm{VA}_{\mathrm{total}}} \quad (18)$$

where P_{TOU} is the output power of the system, V_{total}, G_{total}, and VA_{total} are the total volume, weight, and VA volume of the system, respectively (the volumes and the weights of the power source, the inverter, the rectifier, and the load are not taken into consideration because the comparison focuses on comparing the performances of the switchable-circuit topologies).

Table III lists the comparison among different works. The methods in [17] and [18] require specially designed coils. Thus, compared with these methods, the coil design of the proposed system is easier. However, VSPD, GSPD, and R_{VA} of this letter are smaller than that of Mai *et al.* [17]. For creating once more efficiency-load curve, the cost of switches and passive components in this letter is higher than those in [13], [14], [16], and [17]. However, the reactive power, which increases the power loss and heat, is not introduced by the proposed system. Thus, the proposed method can provide an expandable option for efficiency improvement for an IPT system.

Besides, the methods in [13]–[18] focus on improving the system efficiency in a continuous large load resistance range or a large air gap range. However, the load resistances of a reefer container vary discretely among a few IRPs, and the container is static during operation. Therefore, for the reefer container application, improving the efficiency in a continuous large load resistance range or a large air gap range is unnecessary. Based on this view, the proposed method tries to use a few additional components to optimize efficiency without introducing reactive power. Thus, the proposed method is suitable for the reefer container application.

V. CONCLUSION

In this letter, an SLC-based IPT system is proposed to improve the system efficiency for reefer container wireless charging. The SLC can transform a given load resistance (a larger or smaller resistance than the OLR) into the OLR without introducing extra reactive power. Besides, only a switch, an inductor, and a capacitor are required for creating one more efficiency curve. The experimental results show that the proposed system can gain the system efficiency >92.4% at the IRPs (20 Ω, 259.2 W) and (160 Ω, 32.4 W). Future works may consider using fewer switches and passive components for high-efficiency power transfer. For example, integrating $C_{2,1}$–$C_{2,N}$ ($L_{3,1}$–$L_{3,N}$) into a multiple-tap capacitor (inductor) can further decrease the number of passive components.

REFERENCES

[1] J. Park *et al.*, "A resonant reactive shielding for planar wireless power transfer system in smartphone application," *IEEE Trans. Electromagn. Compat.*, vol. 59, no. 2, pp. 695–703, Apr. 2017.

[2] F. Lu *et al.*, "A tightly coupled inductive power transfer system for low-voltage and high-current charging of automatic guided vehicles," *IEEE Trans. Ind. Electron.*, vol. 66, no. 9, pp. 6867–6875, Sep. 2019.

[3] U. K. Madawala and D. J. Thrimawithana, "A bidirectional inductive power interface for electric vehicles in V2G systems," *IEEE Trans. Ind. Electron.*, vol. 58, no. 10, pp. 4789–4796, Oct. 2011.

[4] Y. Li *et al.*, "A new coil structure and its optimization design with constant output voltage and constant output current for electric vehicle dynamic wireless charging," *IEEE Trans. Ind. Informat.*, vol. 15, no. 9, pp. 5244–5256, Sep. 2019.

[5] Y. Tang, Y. Chen, U. K. Madawala, D. J. Thrimawithana, and H. Ma, "A new controller for bidirectional wireless power transfer systems," *IEEE Trans. Power Electron.*, vol. 33, no. 10, pp. 9076–9087, Oct. 2018.

[6] G. A. Covic, J. T. Boys, M. L. G. Kissin, and H. G. Lu, "A three-phase inductive power transfer system for roadway-powered vehicles," *IEEE Trans. Ind. Electron.*, vol. 54, no. 6, pp. 3370–3378, Dec. 2007.

[7] J. H. Kim *et al.*, "Development of 1-MW inductive power transfer system for a high-speed train," *IEEE Trans. Ind. Electron.*, vol. 62, no. 10, pp. 6242–6250, Oct. 2015.

[8] H. Li, J. Li, K. Wang, W. Chen, and X. Yang, "A maximum efficiency point tracking control scheme for wireless power transfer systems using magnetic resonant coupling," *IEEE Trans. Power Electron.*, vol. 30, no. 7, pp. 3998–4008, Jul. 2015.

[9] W. X. Zhong and S. Y. R. Hui, "Maximum energy efficiency tracking for wireless power transfer systems," *IEEE Trans. Power Electron.*, vol. 30, no. 7, pp. 4025–4034, Jul. 2015.

[10] K. Colak, E. Asa, M. Bojarski, D. Czarkowski, and O. C. Onar, "A novel phase-shift control of semibridgeless active rectifier for wireless power transfer," *IEEE Trans. Power Electron.*, vol. 30, no. 11, pp. 6288–6297, Nov. 2015.

[11] Y. Zhang, T. Kan, Z. Yan, and C. C. Mi, "Frequency and voltage tuning of series–series compensated wireless power transfer system to sustain rated power under various conditions," *IEEE J. Emerg. Sel. Topics Power Electron.*, vol. 7, no. 2, pp. 1311–1317, Jun. 2019.

[12] Y. Li, W. Dong, Q. Yang, J. Zhao, L. Liu, and S. Feng, "An automatic impedance matching method based on the feedforward-backpropagation neural network for a WPT system," *IEEE Trans. Ind. Electron.*, vol. 66, no. 5, pp. 3963–3972, May 2019.

[13] Y. Lim, H. Tang, S. Lim, and J. Park, "An adaptive impedance-matching network based on a novel capacitor matrix for wireless power transfer," *IEEE Trans. Power Electron.*, vol. 29, no. 8, pp. 4403–4413, Aug. 2014.

[14] T. C. Beh, M. Kato, T. Imura, S. Oh, and Y. Hori, "Automated impedance matching system for robust wireless power transfer via magnetic resonance coupling," *IEEE Trans. Ind. Electron.*, vol. 60, no. 9, pp. 3689–3698, Sep. 2013.

[15] J. Kim and J. Jeong, "Range-adaptive wireless power transfer using multiloop and tunable matching techniques," *IEEE Trans. Ind. Electron.*, vol. 62, no. 10, pp. 6233–6241, Oct. 2015.

[16] Z. Dang, Y. Cao, and J. A. Abu Qahouq, "Reconfigurable magnetic resonance-coupled wireless power transfer system," *IEEE Trans. Power Electron.*, vol. 30, no. 11, pp. 6057–6069, Nov. 2015.

[17] R. Mai *et al.*, "Optimization of time-weighted average efficiency for reconfigurable IPT battery charging system," *IEEE Access*, vol. 7, pp. 43092–43099, 2019.

[18] W. Zhong and S. Y. Hui, "Reconfigurable wireless power transfer systems with high energy efficiency over wide load range," *IEEE Trans. Power Electron.*, vol. 33, no. 7, pp. 6379–6390, Jul. 2018.

[19] Y. Chen *et al.*, "Variable-parameter T-circuit-based IPT system charging battery with constant current or constant voltage output," *IEEE Trans. Power Electron.*, vol. 35, no. 2, pp. 1672–1684, Feb. 2020.